Chemistry–A European Journal
Research Article
doi.org/10.1002/chem.202202036
Chemistry Europe
European Chemical Societies Publishing
www.chemeurj.org

A Quick and Reproducible Silanization Method by Using Plasma Activation for Hydrophobicity-Based Kinesin Single Molecule Fluorescence–Microscopy Assays

Viktoria Wedler,[a] Dustin Quinones,[b] Heiko Peisert,[b] and Erik Schäffer*[a]

Abstract: Single-molecule assays often require functionalized surfaces. One approach for microtubule assays renders surfaces hydrophobic and uses amphiphilic blocking agents. However, the optimal hydrophobicity is unclear, protocols take long, produce toxic waste, and are susceptible to failure. Our method uses plasma activation with hydrocarbons for hexamethyldisilazane (HMDS) silanization in the gas phase. We measured the surface hydrophobicity, its effect on how well microtubule filaments were bound to the surface, and the number of nonspecific interactions with kinesin motor proteins. Additionally, we tested and discuss the use of different silanes and activation methods. We found that even weakly hydrophobic surfaces were optimal. Our environmentally friendly method significanty reduced the overall preparation effort and resulted in reproducible, high-quality surfaces with low variability. We expect the method to be applicable to a wide range of other single-molecule assays.

Introduction

The modification of silica-based glass surfaces by silanization has many applications in commercial and scientific areas ranging from the engineering of microelectrodes and sensors, via material bonding and adhesion, to microfluidics, and the immobilization of proteins or other macromolecules to surfaces for single-molecule measurements.[1–14] In particular, for surface-sensitive, single-molecule measurements, high-quality, functional surfaces are necessary.[5,11,15] A broad variety of assays, optimized for many biological assays, have been developed so far (among others[2,5,8–11,13,15]). Yet, as assays are getting more complex and microscopy techniques more sensitive, there is still an ongoing need for assay improvement.

In general, all assays have the same goal of providing sites for specific interaction of certain biomolecules while preventing nonspecific interactions. In so-called kinesin stepping assays, microtubules are first bound to a surface. Subsequently, the translocation of single kinesin motor proteins along microtubules, driven by the motor-catalyzed hydrolysis of adenosine triphosphate (ATP), is tracked using total internal reflection fluorescence TIRF microscopy or optical tweezers. Here, the rigid fixation of microtubules allows an optimal resolution and avoids artifacts due to microtubule motion when measuring kinesin movements.[10,14,15] Moreover, to image and track single kinesin molecules, unspecific interactions with the surface need to be minimized.[2,5,6,11,13–15] Typically, surface-modifications for stepping assays consist of multiple steps and often comprise a basic modification of the glass surface, the adsorption or covalent coupling of different macromolecules for blocking and/or microtubule fixation and sometimes a further modification of the absorbed macromolecules (chemical activation) for microtubule attachment or blocking.[2,5,6,10,11,13,15–17] The overall procedure often requires harsh reagents like piranha solution (sulfuric acid plus hydrogen peroxide) and large amounts of organic solvents. Furthermore, since many steps are involved, it is challenging to reproduce high-quality, functional surfaces.

One popular assay relies on the adsorption of macromolecules to hydrophobic surfaces (Figure 1A).[2,5,9,13,18] In this assay, glass surfaces are rendered hydrophobic by either spin coating with a hydrophobic polymer or a covalent attachment of hydrophobic surface groups via silanization.[2,5,13,18] Subsequently, antibodies against tubulin, for example, anti-β tubulin or in case of modified tubulin anti-rhodamin or anti-biotin, are adsorbed to the surface. For apolar, hydrophobic surfaces, van-der-Waals and hydrophobic interactions mediate the binding of antibodies. They are thought to partially denature on the surface thereby minimizing the overall free energy of the system, i.e. with less water being in contact with the hydrophobic surface.[19–21] The same principle of dehydration of the hydrophobic surface is exploited for passivation of the remaining surface with poloxamers. Poloxamers are triblock copolymers having a hydrophobic polypropylene oxide middle block flanked by two outer, hydrophilic poly(ethylene glycol) (PEG) blocks. In aqueous solutions, poloxamers can form micelles and adsorb onto surfaces.[22] Common poloxamers used for single-

[a] V. Wedler, Prof. Dr. E. Schäffer
Eberhard Karls Universität Tübingen, Cellular Nanoscience (ZMBP), Auf der Morgenstelle 32, 72076 Tübingen, Germany
E-mail: erik.schaeffer@uni-tuebingen.de
[b] D. Quinones, Prof. Dr. H. Peisert
Eberhard Karls Universität Tübingen, Institute of Physical and Theoretical Chemistry, Auf der Morgenstelle 18, 72076 Tübingen, Germany

Supporting information for this article is available on the WWW under https://doi.org/10.1002/chem.202202036

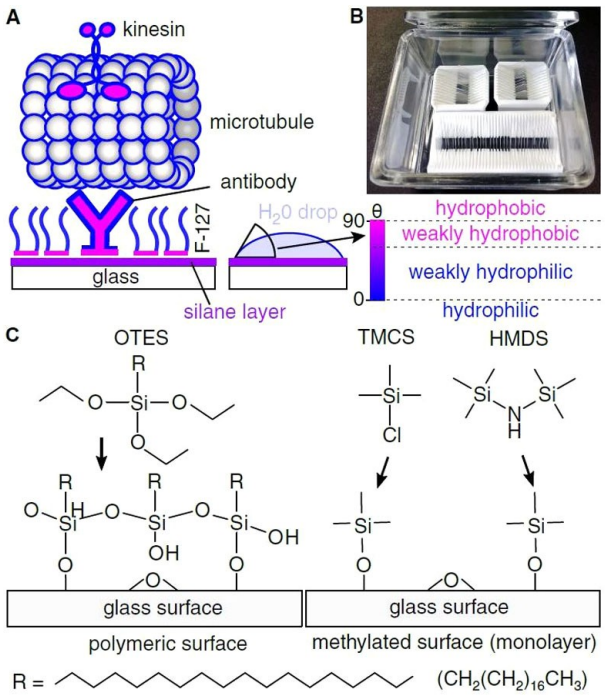

Figure 1. Hydrophobicity-based kinesin assays. A) Scheme of a hydrophobic-interaction-based kinesin assay using antibodies and Pluronic® F-127. Water contact angle θ definitions of hydrophobicity are depicted on the right.[7] B) Image of a glass trough used for cleaning, silanization, and storage. Glass-infused polypropylene (top) and teflon (bottom) racks are shown. C) Polymerizing silanes such as OTES can bridge unhydroxylated sites and impurities, whereas monoreactive silanes such as TMCS and HMDS cannot.

molecule assays are known under the trade name Pluronic® F-127 or F-108 having both 56 propylene oxide units in the middle block and 101 or 129 ethylene oxide units in each of the outer blocks with a PEG molecular weight of 4.4 kD or 5.7 kD, respectively.[2,5,18,23] The hydrophobic middle block adsorbs to the hydrophobic surface while the hydrophilic outer parts protrude into the aqueous solution. If the surface is sufficiently hydrophobic,[24] a polymer brush with a thickness of about 5–10 nm is formed.[18,24,25] This brush passivates the surface against the adsorption of proteins and microspheres.[2,18,25] Instead of poloxamers, smaller amphiphilic molecules, like the polysorbate Tween 20 with 20 ethylene oxide units distributed over four chains, have been used as well.[9] Once the surface is blocked with the poloxamer, microtubules are attached specifically to the respective antibodies and kinesins to the microtubules with minimal binding to the surface.[2]

While the assay itself has been proven to be functional and reliable, silanization reactions are sensitive to various boundary conditions causing erratic failure of protocols.[9,11,26] Also, it is unclear what water contact angle is necessary and optimal. A minimal water contact angle of 90° – the definition of a hydrophobic surface[7] (Figure 1A) – has been reported to be necessary for a "good" assay ($>90°$[13] and $>100°$[5]). Here, we tested various surface activation methods together with three different types of silanes and their suitability for a kinesin stepping assay. To obtain reproducible high-quality functionalized surfaces, we compared and optimized assays while minimizing the overall preparation effort and environmental impact minimizing the use of reagents and organic solvents. For our assay, a water contact angle slightly below 90°, i.e. a weakly hydrophobic surface,[7] was already optimal.

Results and Discussion

Silane choice for coverslip hydrophobization

To measure how the quality of a kinesin stepping assay depends on the water contact angle, we used different surface activation procedures in combination with three silanes. First, coverslips were precleaned in glass troughs (Figure 1B) using a detergent and organic solvent (see the Experimental Section). To improve the silanization efficiency, we subsequently hydroxylated the glass surfaces in an activation step. To this end, we chose two standard cleaning and activation procedures: O_2 plasma activation and HCl etching.[10,13,27] Directly after activation, we silanized the surfaces with three different silane types: octadecyltriethoxysilane (OTES), trimethylchlorosilane (TMCS), and hexamethyldisilazane (HMDS).

Triethoxysilanes like OTES can directly react with a hydroxylated glass surface, i.e. with its silanol groups (Figure 1C left). To fully crosslink the siloxane backbones, often achieved during a curing step at elevated temperatures,[28–30] small amounts of water are necessary. An advantage of polymerizing silanes is that they may bridge unhydroxylated sites[31] (Figure 1C bottom left) or patches of different chemical composition on the surface.[32] Reactions can be catalyzed under acidic or basic conditions or by the addition of amines.[28] In case of the common aminopropyl-triethoxysilane (APTES, $R=C_3H_8N$), the molecule undergoes self catalysis.[28,30] Unfortunately, triethoxysilanes not only polymerize on the surface, but also in solution in the presence of water. If such polymers bind to the surface, the overall surface quality is reduced. Polymerization also occurs in the silane storage container reducing the shelf lifeand reactivity towards surfaces.

Polymerization effects can be avoided by using monofunctional silanes such as TMCS that form a monolayer on glass surfaces (Figure 1C middle). However, in the presence of water, for example through the humidity of air, chlorosilanes also react with each other reducing the overall yield of surface-bound silanes and the shelf lifetime. A promising candidate for more effective and reliable functionalization in a simple lab environment without the generation of polymers is the disilazane HMDS. While the end surface is identical to the monochlorosilanes, HMDS is less sensitive to water and its reactivity towards surface silanol groups is higher because they directly stimulate the decomposition of the disilazane on the surface.[33,34] HMDS silanized surfaces have been shown to work well for the adsorption and characterization of viruses without apparent damage or denaturation due to the adsorption.[35,36] Thus, HMDS is also a good candidate for our antibody-adsorption assay.

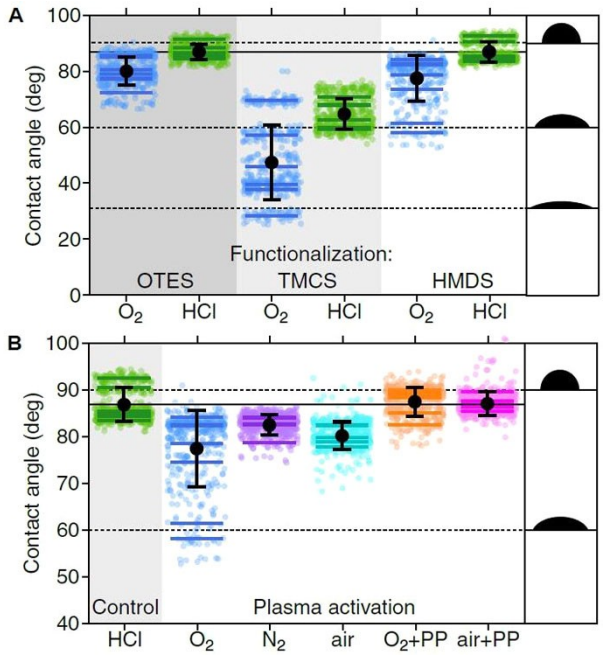

Figure 2. Dependence of the contact angle on activation method and silanes. A) Contact angles on glass surfaces after functionalization with OTES, TMCS and HMDS using either O_2 plasma (blue) or HCl etching (green) activation (individual measurements: small circles, averages of batches: solid lines, overall mean: black circle with SD as error bars). Horizontal dashed lines at 30°, 60° and 90° are drawn with respective droplet silhouettes on the right. B) Contact angles of HCl (green) or O_2 (blue), N_2 (purple), air (cyan), O_2 + PP (orange), and air + PP (magenta) plasma-activated surfaces after HMDS silanization (individual measurements: small circles, averages of batches: solid lines, overall mean: black circle with SD as error bars). A black reference line is drawn through the mean contact angle of the HCl control.

Table 1. Surface composition of elements. Composition (%) of glass surfaces based on the integrated O 1s, Si 2p, C 1s, F 1s, K 2 s, Na 1s, Ti 2p, Zn 2p peaks with major changes marked in bold.

Plasma	O	Si	C	F	K	Na	Ti	Zn
none	54	32	7.4	3.5	2.0	0.7	0.4	0.5
air	**50**	32	6.6	**8.5**	2.1	0.6	0.4	0.4
air + PP	53	33	6.9	4.6	2.0	**0.2**	0.3	0.3

Table 2. Contact angles [°] measured for different activation methods and silanes. Mean ± SD (number of measurements N).

Batch No.	HCl + OTES	O_2 + OTES	HCl + TMCS	O_2 + TMCS	HCl + HMDS
1	86.4 ± 2.8 (72)	72.3 ± 3.5 (72)	67.6 ± 4.5 (72)	28.4 ± 1.4 (50)	92.6 ± 0.7 (72)
2	91.3 ± 1.2 (72)	85.7 ± 2.3 (72)	68.1 ± 4.0 (72)	45.9 ± 3.3 (72)	84.8 ± 1.5 (72)
3	85.6 ± 0.9 (72)	78.8 ± 0.8 (72)	70.8 ± 3.8 (72)	69.7 ± 2.0 (72)	83.4 ± 0.8 (72)
4	85.1 ± 1.0 (72)	80.6 ± 2.5 (72)	62.7 ± 3.6 (72)	39.6 ± 1.9 (72)	85.3 ± 0.8 (72)
5	84.6 ± 2.0 (72)	77.3 ± 1.7 (72)	59.3 ± 1.7 (72)	37.8 ± 2.7 (72)	90.6 ± 1.2 (72)
6	88.3 ± 1.2 (72)	85.2 ± 0.9 (72)	59.9 ± 2.5 (72)	57.3 ± 1.8 (72)	84.4 ± 1.3 (72)
Total	86.9 ± 2.8 (432)	80.0 ± 5.1 (432)	64.7 ± 5.6 (432)	47.4 ± 13.5 (410)	86.9 ± 3.6 (432)

To compare the silanes in our assay, we silanized coverslips from the same batch in parallel with the three silanes and subsequently measured the water contact angle on the coverslips (Figure 2A with individual values of all batches shown in Table 2). In the following, we summarize our findings for the three types of silanes.

Octadecyltriethoxysilane. Based on our previous work with the triethoxysilane APTES,[37] we expected that the use of OTES – having longer hydrocarbon chains compared to APTES – should result in a high water contact angle. HCl-activated slides silanized with OTES had a contact angle of 86.9 ± 2.8° (mean ± SD unless noted otherwise, $N = 432$, Figure 2A) consistent with the literature.[38] Note that for this silanization method and all of the following ones, the variation in contact angles between different batches was usually higher compared to the variation within batches (Table 2 and Table 3). Therefore, we quote the standard deviations and not the standard errors. Compared to HCl etching, the O_2 plasma-treated surfaces had a lower contact angle of 80.0 ± 5.1° ($N = 432$) indicating that O_2 plasma activation was less efficient compared to HCl etching.

Since we did not measure the surface roughness, we do not know whether a change in surface roughness after activation affected the silanization. While plasma activation for 30 s decreased surface roughness,[39] HCl activation is not thought to change the surface roughness even though glass surfaces appear rougher once organic contaminations are removed.[27] KOH activation may be used instead of HCl etching.[37,40] With a short ethanol-KOH incubation time, surface roughness wasreduced.[40] However, if surfaces are kept too long in KOH, surface roughness may increase again. Since sonication in aqueous solutions hydroxylated titanium dioxide and iron oxide surfaces,[41–43] we tested whether sonicating coverslips in pure water was sufficient for hydroxylation. However, sonication in water was not as effective as HCl etching. Nevertheless, all activation methods resulted in hydrophilic surfaces[7] with a zero contact angle such that water was spreading on the coverslips.

Table 3. Contact angles [°] measured for different plasma activation conditions using HMDS. Mean ± SD (number of measurements N).

Batch No.	O_2	O_2 + PP	Air + PP	Air	N_2
1	61.4 ± 5.4 (62)	90.1 ± 1.5 (72)	89.6 ± 2.2 (72)	79.8 ± 2.8 (72)	84.2 ± 1.3 (72)
2	78.6 ± 3.0 (72)	89.1 ± 1.1 (72)	86.4 ± 2.5 (72)	78.9 ± 2.3 (72)	82.6 ± 1.3 (72)
3	84.1 ± 1.4 (72)	89.7 ± 1.2 (72)	86.3 ± 3.4 (72)	79.8 ± 1.7 (72)	82.6 ± 1.1 (72)
4	82.6 ± 1.3 (72)	88.3 ± 1.5 (72)	87.1 ± 1.6 (72)	77.8 ± 1.6 (72)	82.7 ± 1.1 (72)
5	73.5 ± 4.7 (72)	85.1 ± 1.6 (72)	87.6 ± 1.0 (72)	82.6 ± 1.5 (72)	78.8 ± 1.5 (72)
6	82.3 ± 0.7 (72)	82.6 ± 2.1 (72)	85.4 ± 1.0 (72)	82.3 ± 3.9 (72)	84.0 ± 0.9 (72)
7	58.2 ± 11.5 (72)	–	–	–	–
Total	74.6 ± 11.1 (494)	87.5 ± 3.1 (432)	87.1 ± 2.5 (432)	80.2 ± 3.0 (432)	82.5 ± 2.2 (432)

While the contact angle after HCl activation and silanization was high, OTES was very sensitive towards water, the reaction required a lot of solvents and harmful chemicals, solvent exchanges were prone to contaminations, and the protocol was work-intensive. Therefore, we tested silanization methods via the gas phase.

Trimethylchlorosilane. Compared to the OTES silanization, TMCS silanization was more sensitive to the activation procedure. For O_2 plasma and HCl activation, the contact angles were $47 \pm 14^\circ$ ($N = 410$) and $64.7 \pm 5.6^\circ$ ($N = 432$), respectively. These values are much lower than the supposedly required 90° and had a higher variability between batches. Also, contact angles were lower compared to reported values of (i) 85° for a vacuum silanization procedure that emphasized the sensitivity to air humidity[44] and (ii) 70° and 110° for a liquid silanization approach without and with catalyst, respectively.[11] Based on these studies, our low contact angles may be due to remnant air humidity in our desiccator and the absence of a catalyst. We also tested a more reactive trichlorosilane (perfluorodecyltrichlorosilane (FDTS)) with O_2 plasma activation that did not improve the results likely due to its increased sensitivity towards air humidity.[34,45,46] During FDTS experiments, the contact angle meter was not available and contact angles were only assessed by eye to be comparable to the low contact angles observed for TMCS.

Hexamethyldisilazane. HMDS silanization of HCl activated surfaces had a high contact angle of $86.9 \pm 3.9^\circ$ ($N = 432$). The contact angle was lower for the O_2 plasma activated coverslips with a large variation between batches ($75 \pm 11^\circ$, $N = 494$). The dependence on the activation procedure and the high standard deviation of the O_2 plasma treated slides, is consistent with HMDS not being able to polymerize.[33,34]

Overall, HCl activation with OTES or HMDS silanization resulted in comparable contact angles slightly below 90° with a low variability between batches. Nevertheless, as OTES is able to polymerize as its response to ambient air humidity, over a longer term in the laboratory, HMDS was favored. Ambient air humidity solely caused dimerization and thus inactivation of HMDS and thus could be compensated by using HMDS in large excess. Overall, HMDS was less prone to erratic failure in achieving reproducible contact angles. Therefore, we focussed on further optimizing the overall protocol using HMDS.

Optimized plasma surface activation in the presence of hydrocarbons

Even though solution-based activation resulted in higher contact angles with less variability, plasma activation does not produce waste chemicals, is much faster, less sensitive to contaminations, and less work intensive. Therefore, we tested different conditions for plasma activation with subsequent HMDS silanization and measured again water contact angles on the silanized coverslips (Figure 2B). As a control, we plotted the results of the HCl and O_2 plasma activations of Figure 2A (note the zoom-in of the *y*-axis). While the O_2 plasma activation resulted on average in lower contact angles compared to the HCl activation, some batches approached 90° indicating that in principle, plasma activation can achieve a sufficiently high hydroxy density on the surface.[47] In agreement with activation in a N_2 plasma reported to be better,[47] we measured a significantly higher contact angle of $82.5 \pm 2.2^\circ$ ($N = 432$) with less variability when using the N_2 plasma (see Table 4 for significance values). Yet, both O_2 and N_2 plasmas do not contain any hydrogen species for direct surface hydroxylation. Instead, it is assumed that the exposure of the freshly plasma-activated, reactive surfaces to ambient air results in surface-silanol formation.[47] Thus, we tested whether an air plasma with its natural water content would be more effective. However, the contact angle of $80.2 \pm 3.0^\circ$ ($N = 432$) in an air plasma was significantly lower compared to the N_2 plasma. Possibly, the humidity was too low. The direct generation of a water or hydrogen plasma was not possible with our devices.

To generate reactive hydrogen species during plasma activation by decomposition of hydrocarbons,[48,49] we used glass infused polypropylene (PP) racks instead of the teflon racks for the coverslips (Figure 1B). As expected, decompositionof the PP-containing rack caused an increase in the plasma chamber pressure. To keep the pressure constant, we manually compensated this increase by reducing the process gas flow. Also, the color of the plasma flame changed from blue to white. As for any of the other activation methods, after plasma activation, coverslips were hydrophilic with a zero contact angle. Once silanized with HMDS, these O_2+PP treated coverslips had a contact angle of $87.5 \pm 3.1^\circ$ ($N = 432$) – higher and with a lower standard deviation compared to the pure O_2 plasma. Thus, the presence of hydrocarbons during plasma activation improved the hydrophobicity and reproducibility.

One disadvantage of the O_2+PP plasma activation was the rapid degradation of the glass-infused PP racks. This decomposition caused a deformation and surface roughening preventing frequent reuse of the racks (more than three times). Using a lower-power device that generated a homogenous air plasma,

Table 4. Significance of contact angle (CA) differences determined by ANOVA (N = 432, F = 404, $\alpha = 0.01$, confidence interval CI = 99%) with Tukey HSD post hoc. Contact angles were measured for HMDS silanized glass surfaces using different activations. The respective contact angle data can be found in Table 3.

Group 1	Group 2	*p* value	Significantly different
O_2	N_2	$<1\times10^{-13}$	yes
O_2	O_2+PP	$<1\times10^{-13}$	yes
O_2	HCl	$<1\times10^{-13}$	yes
O_2	air+PP	$<1\times10^{-13}$	yes
O_2	air	$<1\times10^{-13}$	yes
N_2	O_2+PP	$<1\times10^{-13}$	yes
N_2	HCl	$<1\times^{-13}$	yes
N_2	air+PP	$<1\times10^{-13}$	yes
N_2	air	10^{-8}	yes
O_2+PP	HCl	0.58	no
O_2+PP	air+PP	0.89	no
O_2+PP	air	$<1\times10^{-13}$	yes
HCl	air+PP	0.99	no
HCl	air	$<1\times10^{-13}$	yes
air+PP	air	$<1\times10^{-13}$	yes
air+PP	HCl+OTES	0.30	no

preserved the racks without visible damage (when used up to ten times). Also, there was no detectable change in the plasma color or chamber pressure. Still, the contact angle of 87.1 ± 2.5° ($N = 432$) was comparable to the pure O_2 + PP plasma with an even lower variability between batches. Instead of the glass-infused PP racks, we tested whether common laboratory items composed of PP or pure PP plates in the plasma cleaner could also improve the activation. However, we did not observe any effect indicating that the improved contact angles were specific to the glass-infused PP racks. Summarizing, the air + PP rack plasma treatment was more robust, simpler and reproducible while maintaining a high contact angle.

The chemical composition hardly depended on the activation method

To understand how the air + PP plasma activation affected the surface chemistry, we performed X-ray photoelectron spectroscopy (XPS) measurements (Figure 3). We compared an air + PP plasma activated coverslip (magenta line) to an untreated, precleanedand an air-plasma-activated coverslip (black and cyan line, respectively). Since the Si 2p and O 1s binding energies that are a signature for surface silanol groups hardly changed, activation did not lead to a significant increase in hydroxylation. Precleaned coverslips may already be well hydroxylated. Based on the elemental surface composition (Table 1), the amount of carbon was small for all surfaces. The carbon content was likely due to exposure of the surfaces to room air.[39] Since the carbon content barely varied between the samples, the air + PP plasma did not deposit any additional hydrocarbons on the surface. Interestingly, for the air plasma, the amount of fluorine roughly doubled with a concurrent reduction in the oxygen peak that we attribute to the use of the PTFE rack. While the contact angles of all three surfaces were hydrophilic after activation, the reduced contact angle after silanization may have been due to fluorine. Thus, we tested air-plasma activation of coverslips without a rack. We found that average contact angles without racks (80.0 ± 2.1 for 5 batches and 360 contact angles) did not differ from the ones with PTFE racks (80.2 ± 3.0, Table 3). Thus, fluorine was not responsible for the lower contact angles. Apart from the change in fluorine, there was a three-fold reduction in sodium for the air + PP plasma activated surfaces. Yet, the total amount of sodium was small. Therefore, we do not expect that the change in sodium content had a major influence on the contact angle after silanization. Overall, the XPS measurements suggest that the air + PP plasma activation did not lead to major chemical surface modifications.

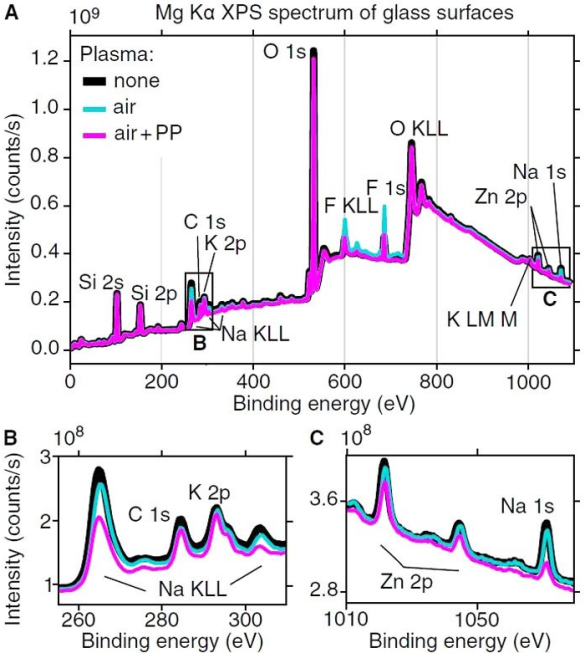

Figure 3. XPS surface analysis. A) XPS spectra of untreated (black line), air plasma (cyan line) and air + PP plasma-activated (magenta line) glass surfaces with peak-assigned elements. Areas outlined with black boxes are enlarged in (B) and (C).

Optimal contact angle for TIRF assays

To determine the optimal contact angle of silanized surfaces for kinesin stepping assays, we measured the signal-to-background ratio (SBR) of motors tagged with green fluorescent protein (GFP) interacting with microtubules by using TIRF microscopy (Figure 4). We quantified the SBR and how well microtubules were attached to the surface as a function of contact angle. All assays were performed on the same day using the same ingredients and kinesin concentration (5 nM). We recorded image stacks of the fluorescent motor actively translocating over microtubules and quantified the ratio between kinesins bound specifically to microtubules and non-specifically to the surface.

Weakly hydrophilic surfaces with a contact angle of about 30° – comparable to that of precleaned, unfunctionalized glass slides, but obtained by an insufficient TMCS silanization – had the lowest SBR (Figure 4A left). Also, microtubules were loosely bound with all ends fluctuating due to Brownian motion. For larger contact angles of about 60°, the SBR nearly quadrupled with half of the microtubule ends being attached (Figure 4A middle). Loose middle parts with attached ends were counted as a loose end as well. The increased SBR was due to a reduced background with the signal not significantly changing (Figure 4B–E, Table 5). Interestingly, the transition to a high-quality

Table 5. SBRs for different contact angles (CA). Signal (S) and background (B, gray values) of kinesin motors binding specifically to microtubules and nonspecifically to the surface, respectively [mean ± SD, (number of measurements)] and their ratio (mean ± propagated SD).

CA	28	61	82	87	93
S	48 ± 7 (7)	43 ± 9 (12)	89 ± 11 (16)	115 ± 22 (16)	81 ± 11 (16)
B	14 ± 3 (16)	3.0 ± 1.4 (16)	2.8 ± 0.8 (16)	2.3 ± 0.5 (16)	1.6 ± 0.5 (16)
SBR	3.5 ± 0.8	13 ± 7	32 ± 10	50 ± 14	50 ± 16

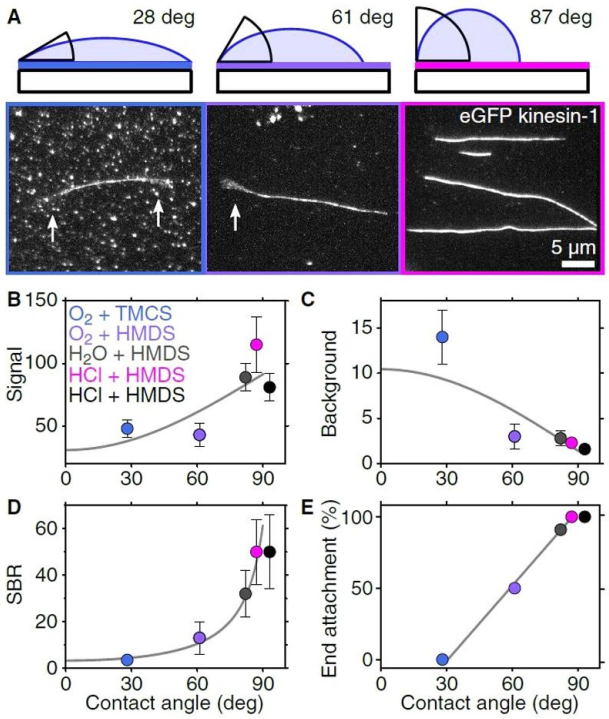

Figure 4. Dependence of the kinesin-stepping assay on the contact angle. A) Maximum projections of kinesin motors walking on microtubules imaged by TIRF microscopy as a function of contact angle. Loose microtubule ends are indicated by arrows. B) Signal, C) background (gray values, mean ± SD), D) signal-to-background ratio (SBR, mean ± propageted SD), and E) percentage of attached microtubule ends as a function of contact angle. A contact-angle model was used to fit the signal, background, and SBR data (lines in B–D, see the Experimental Section). A line with slope 1.76 ± 0.03 and offset −54 ± 3 fits the end attachments in E. The legend in (B) relates the colors of the data points (B–E) and images in A to the activation method used and silane. Note that a different batch was used for the black data points than for the pink ones.

assay in terms of a high SBR with stably attached microtubules occurred for surfaces with a contact angle of 80–90° and not above 90° as suggested previously.[11,13] Therefore, this region was examined in more detail.

Performing the assay on a surface with a contact angle of 80° resulted in a SBR of 32 ± 10 (mean ± propaged standard deviation, $N = 16$) with 90% of the microtubule ends attached. For a contact angle of 80°, the SBR significantly increased to 50 ± 14 ($N = 16$, $p < 0.0001$, Figure 4A right) with all ends attached. For a contact angle of 90°, the SBR did not change (50 ± 16, $N = 16$) with all microtubule ends still attached. While the SBR did not change, the signal significantly decreased ($p < 0.0001$) accompanied by a significant decrease in the background ($p = 0.0004$, Figure 4B–E, Table 5). Up to 90°, the SBR data is well described by a model assuming that kinesins bind nonspecifically to insufficiently blocked parts of the surface (lines in Figure 4B–D, see Experimental). The end attachment percentage is described by a phenomenological linear dependence. Interestingly, in the absence of kinesin motors, all microtubules werewell attached independent of the contact angle. With motors, a proper F-127 polymer brush – forming on surfaces with contact angles above 60°[24] – may be necessary. The brush may prevent competitive binding by shielding the attachment sites of antibodies to microtubules or the surface. The brush thickness increases ith contact angle at least up to 100°.[24] This increase might explain our reduced background with contact angle. If the brush thickness becomes comparable to the distance between the microtubule and the surface (determined by the antibody spacer, see Figure 1A), it may prevent kinesin motors from binding to the bottom of the microtubules. This inhibition may explain the reduction in the microtubule signal. Also, antibodies could denature causing microtubules to be located closer to the surface. An alternative hypothesis, might be that the distance of the microtubule has changed in the evanescent TIRF field. A reduced signal would correspond to an increased microtubule distance from the surface suggesting that a thicker brush may push the microtubules further away from the surface. However, we would expect a similar trend for all of the high-contact angle data which we did not observe. Thus, we favor the hypothesis that the bottom of the microtubule may not be accessible if contact angles are too high. Overall, our results show that contact angles above 90° are not essential for high-quality single-molecule assays but potentially may even be unfavorable.In our experiments, a weakly hydrophobic surface with a contact angle of 87° was already optimal in terms of having a high SBR in combination with the highest signal.

Single-molecule kinesin stepping assays worked well on air-PP-plasma activated HMDS coverslips

To check whether the interaction of motors with microtubules on air + PP plasma activated surfaces silanized with HMDS was comparable to previous studies, we analyzed the motion of single GFP-tagged kinesin-1 motors on these silanized surfaces and determined the motor speed and run length (Figure 5 and Supporting Movie). Consistent with the data in Figure 4, the assay worked reproducibly very well with a high SBR and low autofluorescent background. To determine the motility parameters of single kinesin motors, we generated kymographs showing the position of the kinesin along the microtubule axis as a function of time (Figure 5A). Based on the kymographs and fits to the histograms (Figure 5B), the speed and the run length was 0.8 ± 0.1 µm/s and 0.76 ± 0.04 µm (mean ± fit error, $N = 49$), consistent with our own[14,50,51] and literature

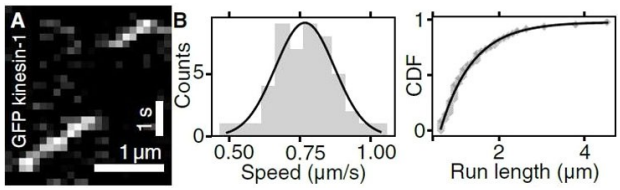

Figure 5. Motility of kinesin-1. A) Exemplary kymograph showing the GFP signal of single kinesin-1 molecules. See the Supporting Movie. B) Histograms of the speed (left) and cumulative distribution function (CDF) of the run length (right) with a Gaussian and exponential fit (lines) to the data.

values.[52,53] Thus, the air + PP plasma activated surfaces did not change the performanceof kinesins and was optimally suited for stepping assays.

Conclusion

We have determined the optimal water contact angle for silanized surfaces used for single-molecule fluorescence kinesin stepping assays. Contrary to previous reports, we found that even weakly hydrophobic surfaces with a contact angle of 87° were optimal. Although a more hydrophobic surface might improve the F-127 polymer brush, a better brush might also block access to the bottom of microtubules or partially denature antibodies. In terms of long-term reliability and reproducibility, the disilazane HMDS turned out to be the best for silanization because it does not polymerize and is less sensitive to humidity. Compared to conventional silanization approaches used for kinesin-single-molecule assays, for which surfaces with a sufficiently high contact angle were only occasionally achieved, all surfaces were of high quality and functional when using our new method. Thus, the assay was more robust and efficient.

To reduce the use of solvents and solutions and reduce the preparation and work effort, the optimal surface activation was via an air plasma with coverslips held in a glass-infused polypropylene rack. This rack presumably provides hydrocarbons that enhance the hydroxylation of the glass surfaces and thereby leads to a high contact angle with low variability after silanization. HMDS silanization only required the addition of silane to the storage glass troughs and an unsupervised incubation in a standard laboratory atmosphere. The plasma activation step also made an organic-solvent-based precleaning step obsolete (see the Experimental Section). The optimized protocol only requires a detergent-based precleaning step with subsequent drying followed by a 5-min plasma activation and then the silanization step. Instead of a full day of work, our new protocol only requires about 30 mins of active work plus the unsupervised incubation time of the surfaces in the presence of HMDS over the weekend. This long incubation time for silanization may be reduced by using a desiccator and vacuum deposition of the silane similar to the TMCS method.[13] The environmentally friendly protocol using a minimal amount of reagents reliably resulted in high-quality surfaces while significantly reducing the overall work load. Therefore, we think that the surfaces are useful for a wide range of single-molecule fluorescence and force measurements.

Experimental

All chemicals were purchased from Sigma Aldrich and used without further purification unless noted otherwise. Purified Type 1 water (18.2 MΩ cm, Nanopure System MilliQ reference with Q-POD and Biopak filter) was used for all experiments. Glass staining jars (BRAND™ 472200 Soda Lime Glass Staining Troughs with Lid, Fisher Scientific, USA with dimensions (L×W×H): 105×85×70 mm on the outside and 91×71×60 mm on the inside) were used to store and treat all coverslips (Figure 1B). Polytetrafluoroethylene (PTFE) racks, custom-made at the university workshop holding up to 20 coverslips, were used to store and handle all coverslips unless noted otherwise. Experiments were performed at room temperature (20–28 °C) unless noted otherwise.

Solvent-based precleaning

Pure white borosilicate glass (D263, hydrolytic class I) coverslips (# 1.5 Corning 22×22 mm^2 and # 0 Menzel 18×18 mm^2 for the bottom and top of the flow cell, respectively) were precleaned. First, coverslips held in PTFE racks were sonicated (Ultrasonic cleaner USC-THD, VWR, US) in a universal detergent (5% Mucasol, Schülke & Mayr GmbH, Norderstedt, Germany) for 3 min and rinsed with water. Racks were rinsed by submerging them in water-filled troughs, taking them out directly afterwards, refilling the trough with fresh water and repeating the process in total three times. Subsequently, coverslips were sonicated for 3 min in acetone and rinsed again with water as described above. This precleaning step takes about 10 min in total. While we used the acetone-cleaning step for all data presented here, it turns out to be unnecessary (data not shown). Currently, we only use the detergent step in our laboratory completely avoiding the use of organic solvents. After the final rinsing step, drying was performed by a combination of blow drying with nitrogen and heating in a 60 °C oven (ULM 500, Memmert, Büchenbarch, Germany). First, larger amounts of water on the coverslips were removed by using a nitrogen or dried-and-filtered-pressurized-air nozzle. Then, coverslips were placed in the oven for 5–20 min followed by a second round of blow-drying and a 5–10-min heating step. As with the acetone-cleaning step, the heating step turned out to be unnecessary. Completely drying the coverslips with dried-and-filtered pressurized air for 5–10 min was sufficient (data not shown). The total time for the drying step was about 30–40 min with heating and 5–10 min without. Together, the precleaning took about 40–50 minor 15–20 min with or without the heating step, respectively.

Surface activation

Plasma-based cleaning and activation was performed directly after the precleaning procedure. A TePla plasma cleaner (Plasma system 100E, PVA TePla AG, Wettenberg, Germany) was used to generate an O_2 (0.7 mbar process gas pressure, 300 W radio frequency (RF) power) and N_2 (0.5 mbar process gas pressure, 300 W RF power) plasma. An air plasma was generated using a Zepto plasma cleaner (Diener, Ebhausen, Germany) with 0.7 mbar process gas pressure and 100 W RF power. To provide hydrocarbons during plasma activation, glass-infused polypropylene (PP) racks (Wash-N-Dry coverslip racks, natural color, WSDR-1000, Diversified Biotech, Doylestown, US) holding 10 coverslips were used instead of the PTFE racks. To keep the process pressure constant, we compensated an increased pressure in the vacuum chamber due to the decomposition of the PP racks in the oxygen plasma by reducing the process gas. To minimize the amount of process gas reacting with the plasma activated surface after plasma cleaning using the PP racks, the process gas valve was closed within milliseconds. The plasma cleaning duration was always 5 min. Including time for sorting the coverslips from the PTFE to the PP rack and back and adjusting the plasma cleaner settings, the total time for the plasma cleaning step was less than 10 min.

HCl-based hydroxylation was done as described previously[13] but using O_2 plasma cleaned glass slides. Briefly, slides were immersed in 1 M HCl and sonicated for 90 min. During this time, the coverslips were heated to 75 °C within30 min and further sonicated at 75 °C for 60 min. Sonicating coverslips in pure water was done with the

same sonication and temperature conditions as above. Subsequently, coverslips were rinsed in water and dried as described above adding another 40 min to the procedure. The total time for HCl activation was about 130 min.

Most surface preparations and contact angle measurements have been performed in a clean room facility. All air-plasma based measurements and kinesin measurements have been performed in a standard biochemical laboratory.

Silanization

Cleaned, activated, and dried coverslips were silanized with either (i) octadecyltriethoxysilane (OTES), (ii) trimethylchlorosilane (TMCS) or (iii) hexamethyldisilazane (HMDS). (i) OTES binding was similar to.[38] Coverslips were submerged in a mixture of 200 mL toluene, 4 mL OTES (abcr, Karlsruhe, Germany) and 1 mL *n*-butylamine (nBuNH$_2$) as catalyst for 90 min. To remove residual chemicals, the slides were rinsed in toluol, sonicated for 3 min in acetone, and subsequently rinsed in water and dried using dried, filtered pressurized air. (ii) For TMCS silanization, 800 μL of TMCS were evaporated in a desiccator by alternating intervals of vacuum generation (20 mbar, PC 3004 Vario with CVC 3000 display, Vacuubrand, Wertheim, Germany) and incubation as described earlier.[13] Coverslips were exposed to the TMCS vapour for about 30–40 min in total. (iii) HMDS silanization was similar to.[54] We added 4.5 mL HMDS to the bottom of the glass staining troughs containing the activated coverslips in PTFE racks and left them undisturbed for 48 h with the lid closed. While the incubation time is long, no vacuum, monitoring, or other work steps were required. For storage, we sealed the lid with parafilm. To this end, the lid does not have to be opened after the incubation if coverslips are only used at a later point in time. Silanized slides couldbe stored for several weeks without reducing assay performance.

Microtubule polymerization and taxol stabilization

Porcine tubulin (25 μM) was polymerized in PEM buffer (80 mM PIPES, 1 mM EGTA, 1 mM $MgCl_2$, pH = 6.9) supplemented with 4 mM $MgCl_2$ and 1 mM GTP for 30 min at 37 °C as described previously.[55] Afterwards, the microtubule solution was diluted (1 : 40) in PEM–T (PEM buffer with 1% paclitaxel also called Taxol®), centrifuged (Airfuge Beckman Coulter, Brea, CA), and resuspended in 150 μL PEM–T. Note that microtubules did not contain any fluorescent labels. Thus, microtubules were visualized with label-free interference reflection microscopy (IRM).[56,57] When decorated with fluorescently-tagged kinesin motors, a custom-built TIRF microscope[58] was used.

Flow cell preparation and motility assay

Silanized coverslips were used to build flow cells. Two spacers of double sticky tape (Tesa, part of Hexagon AB, Stockholm, Sweden) connected the bottom and the top slide defining a flow channel between them. Microtubule attachment, surface passivation, and kinesin assays were performed as explained previously,[55] but reducing incubation times with the antibodies and F-127. Also, we used dithiothreitol (DTT) instead of β-mercaptoethanol and the enhanced green fluorescent protein (eGFP)-labeled kinesin 1 (rk430-eGFP-His6).[59] To fill the channel of the hydrophobic flow cell with aqueous solution in the first step, vacuum suction was briefly applied to one end of the channel. For all further liquid exchanges, dry filter paper was used at one end of the channel to fill in other solutions. First, 10 μL anti-tubulin antibody (2 mg/mL) were flown in and allowed to bind for 3 min. Then, 20 μL Pluronic® F-127 (1% in PEM) was used for 10 min. Subsequently, the flow cell was washed 4× with PEM buffer and once with PEM–T. Afterwards, 10 μL taxol-stabilized microtubules were allowed to bind for 10 s and unbound microtubules were washed out with 20 μL PEM–T buffer. Finally, 10 μL of kinesin-1 was diluted to 5 nM for signal-to-background-ratio measurements and to 0.5 nM for single-molecule tracking assays in motility buffer (PEM–T, 0.08 mg/mL casein, 1 mM ATP, 20 mM D-glucose, 250 nM glucose oxidase, 134 nM catalase, 10 mM DTT in PEM buffer) and imaged. For single-molecule tracking assays, after a short incubation step, unbound kinesins were washed out with 5 μL motility buffer.

Microscopy

TIRF microscopy images were recoreded at room temperature (23 °C) on a setup combining IRM and TIRF microscopy.[58] The TIRF excitation wavelength was 488 nm (100 mW LuxX 488–100 Omicron Laser, Rodgau, Germany). The image acquisition time was 200 ms using an Orca Flash 4.0 V2 camera (Hamamatsu Photonics, Hamamatsu City, Japan). The high contrast of TIRM microscopy allowed to image single GFP-tagged kinesins motors. For IRM illumination, a blue LED (Royal-Blue LUXEON Rebel LED, Lumileds, Germany) with an emission wavelength of $\lambda = 450 \pm 20$ nm was operated at 3 V and a current of 0.1 A. IRM imaging was performed with a CCD camera (LU135-M, Lumenera, Canada) at 60 frames per second (fps).

Signal-to-background ratio (SBR) determination

Image stacks contained 100 TIRF images from which we calculated a maximum projection. From these stacks, 40 pixel long straight line segments of microtubules were chosen and 40×40 pixel regions of interest (ROIs) were centered around these line segments using a custom-written tool in Fiji.[60] Multiple ROIs from different sections and microtubules were averaged. From the average ROI, an average profile perpendicular to the microtubule axis was calculated using a custom Python script.[56] The maximum intensity of the average profile minus the dark signal of the camera was used as the microtubule signal. To determine the background intensity, we averaged the 100 TIRF images. From the average pixel value of a 100×100 pixel ROI of a microtubule-free region, we subtracted the dark signal of the camera resulting in the background signal. The ratio of the microtubule to the background signal resulted in the SBR.

Kinesin motility parameters

Kymographs of the TIRF image stacks were generated using Fiji.[60] Line profiles along the microtubule as a function of time are stacked on top of each other such that position along the microtubule corresponds to the *x*-axis and time to the *y*-axis of the kymograph. Kinesin traces shorter than 4 pixels were excluded from the analysis because they could not clearly be identified as processive motion. Kinesin traces that appeared to be due to the movement of multiple kinesins (clusterslarger than a diffraction-limited spot, brightness much higher than that expected for the two-GFP molecules the dimeric kinesin has, partial bleaching) were excluded as well. Speed and run length were determined based on the slope and horizontal projection of lines manually matched to the kinesin traces using Fiji.[60]

Contact angle measurements

Static contact angle measurements were performed at a temperature of 23–25 °C using the sessile drop method on a CAM 200 optical angle meter (KSV Instruments LTD, Helsinki, Finland). The drop volume was 2 μL. Typically, 12 droplets were measured per surface. Three surfaces were measured resulting in 36 contact angles per batch. Six batches were measured per method on different days. As no systematic difference was visible between left and right contact angles, all measured angles were included. Statistical significance was tested by a one-way ANOVA with Tukey HSD post-hoc test with a confidence level of $\alpha = 0.01$ using the Real Statistics Data Analysis Tool in Excel (Microsoft).

Contact angle dependence of the signal-to-background ratio

According to Cassie's equation,[61] the effective contact angle (CA) of a liquid on a flat surface composed of two chemically different components with area fraction $f_{1,2}$ and contact angle $\theta_{1,2}$ is given by

$$cos\mathrm{CA} = f_1 cos\theta_1 + f_2 cos\theta_2. \quad (1)$$

In our assay, the contact angle of an activated, hydroxylated surface was $\theta_1 = 0°$. We assumed that silanization added a hydrophobic surface fraction f_2 with a contact angle of $\theta_2 = 90°$. The relative proportions of f_1 and f_2 were assumed to determine the effective contact angle according to Eq. 1. Inserting θ_1 and θ_2 into Eq. 1, directly relates the effective contact angle to the hydrophilic area fraction f_1

$$cos\mathrm{CA} = f_1. \quad (2)$$

The total number of kinesins N_t in the flow cell, is given by the number of motors in solution plus the number of kinesins attached to microtubules N_{MT} and the number of kinesins that attach nonspecifically to the surface. The number of microtubule-bound motors is proportional to the landing rate that in turn is proportional to the concentration of motors in the solution. We assume that the number of nonspecifically bound motors scales with the insufficiently silanized area fraction f_1 that is poorly blocked by F-127. Based on these assumptions, the microtubule-bound number of kinesins is

$$N_{MT} = a(N_t - N_S f_1), \quad (3)$$

where N_S is the maximum number of nonspecifically bound kinesins and a a proportionality constant. We expect the SBR of an unlabeled microtubule decorated with kinesins to be the ratio of the number of microtubule-bound motors N_{MT} to the nonspecifically bound motors $N_S f_1$. Note that in the following, these are normalized number densities resulting in a certain fluorescence level of a cross-section perpendicular to a microtubule. Additionally, we included a contact-angle-independent background fluorescence *Bkg*, for example, due to autofluorescence resulting in

$$\mathrm{SBR} = \frac{N_{MT}}{N_S f_1 + Bkg}. \quad (4)$$

Inserting Eq. 2 and Eq. 3 into Eq. 4, relates the SBR to the contact angle

$$\mathrm{SBR} = a\frac{N_t - N_S cos\mathrm{CA}}{N_S cos\mathrm{CA} + Bkg}. \quad (5)$$

We fitted these equations to the signal, background and SBR data up to CA = 90° (gray lines in Figure 4B–D) resulting in the following global fit parameters: $a = 2.3 \pm 1.8$, $N_t = 30.9 \pm 19.0$, $N_S = 13.3 \pm 3.7$, and $Bkg = 1.0 \pm 0.7$. Based on the ratio of N_S to N_t, about 65% of the kinesins bound to an untreated surface ($f_1 = 1$ or CA = 0). The model is only valid up to CA = 90° and does not consider a denaturation effect of the antibodies, a polymer brush transition as a function of CA, or other factors that are expected to lead to a saturation effect.

XPS measurements

X-ray photoelectron spectroscopy (XPS) measurements were performed using a multi-chamber ultrahigh vacuum system (base pressure below 8×10^{-10} mbar) including a Phoibos 100 analyzer, a 1d-Delay Line detector (SPECS, Germany) and an X-ray source with a conventional Al/Mg anode (XR-50 X-ray source). All measurements were performed with Mg Kα radiation ($h\nu = 1253.6$ eV), a pass energy of 50 eV, a step size of 0.5 eV, a dwell time of 0.2 s, and a range of −5–1100 eV. The shifts observed due to charging effects of the glass surface were corrected such that the distance between the C1s and the O1s peak were identical for all samples. To determine the elemental composition peak areas were calculated using Python. The slope of the background was calculated for each peak locally. To obtain the atomic percentages, peak areas were weighted with Yeh and Landau sensitivity factors.[62]

Author Contributions

V.W. planned and performed the experiments. D.Q. and V.W. performed and analyzed XPS measurements. H.P. supervised and contributed to the XPS analysis. V.W. and E.S. analyzed the data, and wrote the manuscript.

Supplementary Movie

Motility of kinesin-1. Single GFP-tagged kinesins (green) walking on microtubules (magenta). The superposition and colocalization of kinesins on microtubules makes walking kinesins appear white. The green background is mainly due to the camera background. The video is real-time with 5 frames per second. The kymograph of the video is shown in Figure 5.

Acknowledgements

We thank Sebastian Kenzler, Anita Jannasch, Hauke Drechsler, and Carolina Carrasco for comments on the manuscript, the LISA + center for plasma cleaner usage and the clean room, and Thomas Chassé for help with the XPS measurements. This work was supported by the interdisciplinary "nanoBCP-Lab" funded by the Carl Zeiss Foundation and the PhD Network "Novel Nanoparticles" of the Universität Tübingen. Open Access funding enabled and organized by Projekt DEAL.

Conflict of Interest

The authors declare no conflict of interest.

Data Availability Statement

The data that support the findings of this study are available from the corresponding author upon reasonable request.

Keywords: Surface chemistry · single-molecule fluorescence · silanes · photoelectron spectroscopy · microtubules

[1] J.-L. Munoz, F. Deyhimi, J. Coles, *J. Neurosci. Methods* **1983**, *8*, 231.
[2] J. Helenius, G. Brouhard, Y. Kalaidzidis, S. Diez, J. Howard, *Nature* **2006**, *441*, 115.
[3] J. Matinlinna, P. Vallittu, *J. Oral Rehabil.* **2007**, *34*, 622.
[4] J. Blümmel, N. Perschmann, D. Aydin, J. Drinjakovic, T. Surrey, M. Lopez-Garcia, H. Kessler, J. P. Spatz, *Biomaterials* **2007**, *28*, 4739.
[5] "Microtubule Dynamics Reconstituted in Vitro and Imaged by Single-Molecule Fluorescence Microscopy", C. Gell, V. Bormuth, G. J. Brouhard, D. N. Cohen, S. Diez, C. T. Friel, J. Helenius, B. Nitzsche, H. Petzold, J. Ribbe, E. Schäffer, J. H. Stear, A. Trushko, V. Varga, P. O. Widlund, M. Zanic, J. Howard in *Methods in Cell Biology, Vol. 95: Microtubules, in Vitro* (Eds.: L. Wilson, J. J. Correia), Academic Press, San Diego, **2010**, Chapter 13.
[6] "Fluorescence Microscopy Assays on Chemically Functionalized Surfaces for Quantitative Imaging of Microtubule, Motor, and +TIP Dynamics", P. Bieling, I. A. Telley, C. Hentrich, J. Piehler, T. Surrey in *Methods in Cell Biology, Vol. 95: Microtubules, in Vitro* (Eds.: L. Wilson, J. J. Correia), Academic Press, San Diego, **2010**, Chapter 28.
[7] J. Drelich, E. Chibowski, D. D. Meng, K. Terpilowski, *Soft Matter* **2011**, *7*, 9804.
[8] A. Yildiz, N. Forkey Joseph, A. McKinney Sean, T. Ha, E. Goldman Yale, R. Selvin Paul, *Science* **2003**, *300*, 2061.
[9] B. Hua, K. Y. Han, R. Zhou, H. Kim, X. Shi, S. C. Abeysirigunawardena, A. Jain, D. Singh, V. Aggarwal, S. A. Woodson, T. Ha, *Nat. Methods* **2014**, *11*, 1233.
[10] "Covalent Immobilization of Microtubules on Glass Surfaces for Molecular Motor Force Measurements and Other Single-Molecule Assays", M. P. Nicholas, L. Rao, A. Gennerich in *Mitosis*, Springer, **2014**, pp 137–169.
[11] M. Szkop, B. Kliszcz, A. A. Kasprzak, *Anal. Biochem.* **2018**, *549*, 119.
[12] A. Shakeri, N. A. Jarad, A. Leung, L. Soleymani, T. F. Didar, *Adv. Mater. Interfaces* **2019**, *6*, 1900940.
[13] W. G. Hirst, C. Kiefer, M. K. Abdosamadi, E. Schäffer, S. Reber, *STAR protocols* **2020**, *1*, 100177.
[14] S. Sudhakar, M. K. Abdosamadi, T. J. Jachowski, M. Bugiel, A. Jannasch, E. Schäffer, *Science* **2021**, *371*, eabd9944.
[15] S. Sudhakar, T. J. Jachowski, M. Kittelberger, A. Maqbool, G. L. Hermsdorf, M. K. Abdosamadi, E. Schäffer, *Nano Lett.* **2019**, *19*, 8877.
[16] R. D. Vale, T. S. Reese, M. P. Sheetz, *Cell* **1985**, *42*, 39.
[17] J. Howard, A. J. Hunt, S. Baek, *Methods Cell Biol.* **1993**, *39*, 137.
[18] E. Schäffer, S. F. Nørrelykke, J. Howard, *Langmuir* **2007**, *23*, 3654.
[19] M. E. Wiseman, C. W. Frank, *Langmuir* **2012**, *28*, 1765.
[20] L.-C. Xu, C. A. Siedlecki, *Biomaterials* **2007**, *28*, 3273.
[21] R. G. Couston, M. W. Skoda, S. Uddin, C. F. van der Walle, *mAbs* **2013**, *5*, 126.
[22] P. Alexandridis, T. Alan Hatton, *Colloids Surf. A* **1995**, *96*, 1.
[23] L.-J. Cheng, M.-T. Kao, E. Meyhöfer, L. J. Guo, *Small* **2005**, *1*, 409.
[24] M. R. Nejadnik, A. L. J. Olsson, P. K. Sharma, H. C. van der Mei, W. Norde, H. J. Busscher, *Langmuir* **2009**, *25*, 6245.
[25] W. Norde, D. Gage, *Langmuir* **2004**, *20*, 4162.
[26] J. Brzoska, I. B. Azouz, F. Rondelez, *Langmuir* **1994**, *10*, 4367.
[27] H. K. Jang, Y. D. Chung, S. W. Whangbo, I. W. Lyo, C. N. Whang, S. J. Lee, S. Lee, *J. Vac. Sci. Technol. A* **2000**, *18*, 2563.
[28] F. Osterholtz, E. Pohl, *J. Adhes. Sci. Technol.* **1992**, *6*, 127.
[29] G. L. Witucki, *J. Coat. Technol.* **1993**, *65*, 57.
[30] P. van der Voort, E. Vansant, *J. Liq. Chromatogr. Relat.* **1996**, *19*, 2723.
[31] A. V. Krasnoslobodtsev, S. N. Smirnov, *Langmuir* **2002**, *18*, 3181.
[32] H. Cai, S. J. Wind, *Langmuir* **2016**, *118*, 10034.
[33] M. Hair, W. Hertl, *J. Phys. Chem.* **1971**, *75*, 2181.
[34] M. Hair, C. Tripp, *Colloids Surf. A: Physicochem. Eng. Asp.* **1995**, *105*, 95.
[35] I. L. Ivanovska, P. J. de Pablo, B. Ibarra, G. Sgalari, F. C. MacKintosh, J. L. Carrascosa, C. F. Schmidt, G. J. L. Wuite, *Proc. Natl. Acad. Sci. USA* **2004**, *101*, 7600.
[36] C. Carrasco, A. Carreira, I. A. T. Schaap, P. A. Serena, J. Gómez-Herrero, M. G. Mateu, P. J. de Pablo, *Proc. Natl. Acad. Sci. USA* **2006**, *103*, 13706.
[37] V. Wedler, F. Strauß, S. Sudhakar, G. L. Hermsdorf, Y.-D. Stierhof, E. Schäffer, *Nanoscale Adv.* **2020**, *2*, 4003.
[38] D. M. Walba, C. A. Liberko, E. Korblova, M. Farrow, T. E. Furtak, B. C. Chow, D. K. Schwartz, A. S. Freeman, K. Douglas, S. D. Williams, et al., *Liq. Cryst.* **2004**, *31*, 481.
[39] K. Terpilowski, D. Rymuszka, *Glass Phys. Chem.* **2016**, *42*, 535.
[40] N. Chada, K. P. Sigdel, R. R. S. Gari, T. R. Matin, L. L. Randall, G. M. King, *Sci. Rep.* **2015**, *5*, 12550.
[41] A. Henglein, *Ultrasonics* **1987**, *25*, 6.
[42] C. Yang, G. Wang, Z. Lu, J. Sun, J. Zhuang, W. Yang, *J. Mater. Chem.* **2005**, *15*, 4252.
[43] N. Sakai, R. Wang, A. Fujishima, T. Watanabe, K. Hashimoto, *Langmuir* **1998**, *14*, 5918.
[44] W. J. Herzberg, J. E. Marian, T. Vermeulen, *J. Colloid Interface Sci.* **1970**, *33*, 164.
[45] L. Shaffer, E. Flanigen, *J. Phys. Chem.* **1957**, *61*, 1595.
[46] M. L. Hair, W. Hertl, *J. Phys. Chem.* **1969**, *73*, 2372.
[47] L. Pasternak, Y. Paz, *RSC Adv.* **2018**, *8*, 2161.
[48] W. Petasch, B. Kegel, H. Schmid, K. Lendenmann, H. Keller, *Surf. Coat. Technol.* **1997**, *97*, 176.
[49] S. Ahmed, A. Aitani, F. Rahman, A. Al-Dawood, F. Al-Muhaish, *Appl. Catal. A* **2009**, *359*, 1.
[50] M. Bugiel, E. Böhl, E. Schäffer, *Biophys. J.* **2015**, *108*, 2019.
[51] A. Ciorîţă, M. Bugiel, S. Sudhakar, E. Schäffer, A. Jannasch, *Cytoskeleton* **2021**, *78*, 177.
[52] S. M. Block, L. S. Goldstein, B. J. Schnapp, *Nature* **1990**, *348*, 348.
[53] D. L. Coy, M. Wagenbach, J. Howard, *J. Biol. Chem.* **1999**, *274*, 3667.
[54] A. Kawai, J. Kawakami, *J. Photopolym. Sci. Technol.* **2003**, *16*, 665.
[55] M. Chugh, M. Reißner, M. Bugiel, E. Lipka, A. Herrmann, B. Roy, S. Müller, E. Schäffer, *Biophys. J.* **2018**, *115*, 375.
[56] S. Simmert, M. K. Abdosamadi, G. Hermsdorf, E. Schäffer, *Opt. Express* **2018**, *26*, 14499.
[57] M. Mahamdeh, S. Simmert, A. Luchniak, E. Schäffer, J. Howard, *J. Microsc.* **2018**, *272*, 60.
[58] A. K. Schellhaus, D. Moreno-Andrés, M. Chugh, H. Yokoyama, A. Moschopoulou, S. De, F. Bono, K. Hipp, E. Schäffer, W. Antonin, *Sci. Rep.* **2017**, *7*, 9996.
[59] A. Ramaiya, B. Roy, M. Bugiel, E. Schäffer, *Proc. Natl. Acad. Sci. USA* **2017**, *114*, 10894.
[60] J. Schindelin, I. Arganda-Carreras, E. Frise, V. Kaynig, M. Longair, T. Pietzsch, S. Preibisch, C. Rueden, S. Saalfeld, B. Schmid, J.-Y. Tinevez, D. J. White, V. Hartenstein, K. Eliceiri, P. Tomancak, A. Cardona, *Nat. Methods* **2012**, *9*, 676.
[61] A. B. D. Cassie, *Discuss. Faraday Soc.* **1948**, *3*, 11.
[62] J. Yeh, I. Lindau, *At. Data Nucl. Data* Tables **1985**, *32*, 1.

Manuscript received: June 30, 2022
Accepted manuscript online: August 4, 2022
Version of record online: September 14, 2022